JOURNAL OF SOLID STATE CHEMISTRY 84, 194–210 (1990)

Structural Aspects of the α Transition in Stoichiometric FeS: Identification of the High-Temperature Phase

F. KELLER-BESREST* AND G. COLLIN

Unité associée au CNRS No. 200, Université René Descartes, 4 avenue de l'Observatoire, 75006 Paris, France

Received March 15, 1988; in revised form July 12, 1989

Compounds of the $Fe_{1-x}S$ system ($0 \leq x \leq 0.125$) are of NiAs type (a and c being the substructure lattice constants). For $0 \leq x \leq 0.05$, the temperature-induced metal–nonmetal α transition is associated with a structural change. Powder studies identify the influence of x on the transition and especially on the superstructure reflection intensities of the hexagonal $\sqrt{3}a,2c$ low-temperature ($T < T_\alpha$) phase. Crystal growth for compositions in the transition range is detailed. The structural study of a stoichiometric FeS crystal at various temperatures gives evidence for disorder phenomena in the pretransition range and for the exact nature of the hexagonal HT phase ($T > T_\alpha$) $2a,c$ (SG $P6_3mc$). Its structure refinement ($R = 6.0\%$) rules out the previous tritwinned model of *MnP* type. The cationic lattice of this $2a,c$ modification is intermediate between the lattices of the LT $\sqrt{3}a,2c$ phase and those of a pure NiAs phase.

I. Introduction

The $Fe_{1-x}S$ system is noteworthy for its large possible cation deficiency which gives rise to a solid solution from FeS to Fe_7S_8 ($Fe_{0.875}S$). Introduction of vacancies leads to a variety of magnetic and electrical properties, extensively studied in relation to structural analysis.

Like many of the $3d$ transition metal chalcogenides, the $Fe_{1-x}S$ compounds belong to the NiAs structural type. The ideal hexagonal elementary cell (a,c lattice constants; $Z = 2$; SG:$P6_3/mmc$) is illustrated in Fig 1. It consists of an *hcp* lattice of S atoms with Fe atoms inserted in the octahedral sites, following the stacking sequence *ABAC*. . . . One of the main interests of the $Fe_{1-x}S$ system is the existence of a first-order phase transition (conventionally named the α transition) which occurs on the iron-rich side at a temperature, T_α, of 147°C for FeS. Extensive structural and physical investigations reported recently (*1–4*) agree on the following main characteristics:

—At low temperature (LT), $T < T_\alpha$, the conductivity σ is that of a semiconductor, but its dependence on T cannot be fitted to a classical law.

—At the transition and with a composition close to FeS, σ increases by two order of magnitude and for $T > T_\alpha$ still increases slowly with T. The high-temperature (HT) phase is often described as a poor, highly correlated metal.

—In the whole temperature range, the conductivity is p type and the compound

* To whom all correspondance should be addressed.

0022-4596/90 $3.00

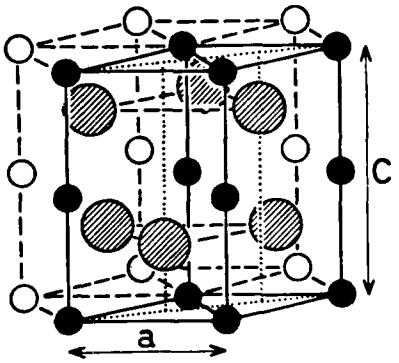

FIG. 1. The NiAs cell. Small circles represent metallic atoms (0;0;0 and 0;0;½) and large circles correspond to nonmetallic atoms (⅔;⅓;¼) and (⅓;⅔;¾).

remains antiferromagnetically ordered up to T_N = 327°C, with a discontinuity of the susceptibility at T_α.

The characteristics of the transition are highly dependent on the vacancy rate x, and the transition is suppressed for high x values.

The crystallographic phase transition associated with the change in electronic structure has been investigated. The LT phase is a hexagonal superstructure of an NiAs-type cell, with lattice constants $\sqrt{3}a,2c$ (*5*). Iron atoms are displaced from the NiAs positions by small shifts perpendicular to c and form triangular clusters in the hexagonal plane. The HT phase has not yet been clearly identified. In other respects, the influence of vacancies on the physical characteristics of the transition has been evaluated. But the defect of the previous work comes from the lack of structural data concerning the evolution of the lattice with respect to T or x. This originates from the difficulty of getting well-characterized $Fe_{1-x}S$ crystals in the composition range of the α transition.

In this first paper, we present the method of synthesis and characterization of $Fe_{1-x}S$, particularly stoichiometric FeS single crystals which allow a complete description of the crystallographic transition:

—Identification of the exact nature of the HT phase as a hexagonal superstructure $2a,c$, in opposition to a recently proposed *MnP*-type twinned model (*6*).

—Analysis of the process of weakening of both types of superstructures as originating from disorder phenomena.

The influence of vacancies on the structural aspect of the transition will be analyzed in detail in a second paper devoted to the study of $Fe_{0.985}S$ and $Fe_{0.975}S$ single crystals (*7*).

These studies concern the transition in cation-deficient $Fe_{1-x}S$ compounds. Another approach to this transition is based on the study of $Fe_{1-x}M_xS$ compounds where vacancies are substitued by M = Cr, Mn, or Co (*8*, *9*). These substitutions with 3*d* elements produce cations acting like more or less charged impurities, as opposed to purely vacant Fe sites in $Fe_{1-x}S$ compounds. From this work emerges an interpretation of the α transition as resulting from a polaron mechanism.

II. Study on Powders

(*A*) *Synthesis*

Numerous materials with compositions ranging from FeS to Fe_7S_8 are prepared with special care to control the vacancy rate. First, large quantities of FeS and Fe_7S_8, which are the defined compounds of the phase diagram, are prepared from elements (Fe previously reduced in hydrogen). Then, $Fe_{1-x}S$ samples are obtained from a mixture in the desired proportions of FeS and Fe_7S_8 powders. At each stage of the synthesis, the products are heated in a graphite crucible inside an evacuated silica–glass tube at 660°C for 2 weeks. To ensure the homogeneity of the powders, after quenching, the products are ground and again heated at high temperature.

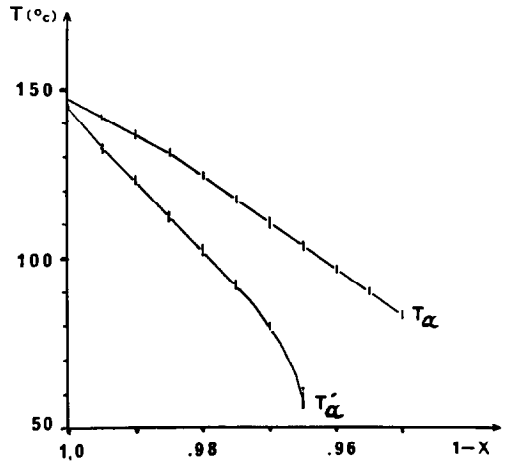

FIG. 2. Transition temperature, from LT to HT (T_α) and from HT to LT (T'_α) versus $(1-x)$.

ing and splitting of some substructure reflections, particularly when x is higher. For compositions close to $Fe_{0.95}S$, the powders are mixtures of phases as soon as they are quenched.

—From Fig. 3 one observes that nonstoichiometry influences mainly the c axis ($\Delta c/\Delta x = -0.015$ Å$(\%x)^{-1}$) and a versus x varies in opposite directions on both sides of the $Fe_{0.95}S$ composition.

These powder studies show that $x_{lim} = 0.05$ delimits two parts in the FeS–Fe_7S_8S phase diagram:

—The α transition range ($0 < x < x_{lim}$) with a gradual weakening of the LT $\sqrt{3}a,2c$ superstructure reflections.

(B) *Study of the Transition Range*

$Fe_{1-x}S$ powders are simultaneously subjected to Guinier–Lainé X-ray study (Cu$K\alpha$) and differential thermal analysis (DTA). Figure 2 shows the dependence of the transition temperature on x and Figure 3 presents the gradual change of the NiAs substructure lattice constants a and c (refined by least-square methods).

The $T_\alpha = f(x)$ curve shows that the transition exists for the compositional range FeS–$Fe_{0.95}S$. When x increases:

—T_α decreases ($\Delta T_\alpha/\Delta x = -14$°C$(\%x)^{-1}$) and the amplitudes of the DTA peaks of the transition decrease and spread over a large temperature range.

—The hysteresis ΔT, which is 4°C for FeS, increases rapidly ($\Delta(\Delta T)/\Delta x = 8.7$°C$(\%x)^{-1}$) and the processes spread over a larger temperature range. It is no longer observable when $x > 0.035$.

—The intensity of the reflections of the $\sqrt{3}a,2c$ superstructure decreases, and they are no longer observable for $x > x_{lim} = 0.05$. From $x = 0.01$, this weakening is accompanied by the progressive appearance of a phase mixture as revealed by the broaden-

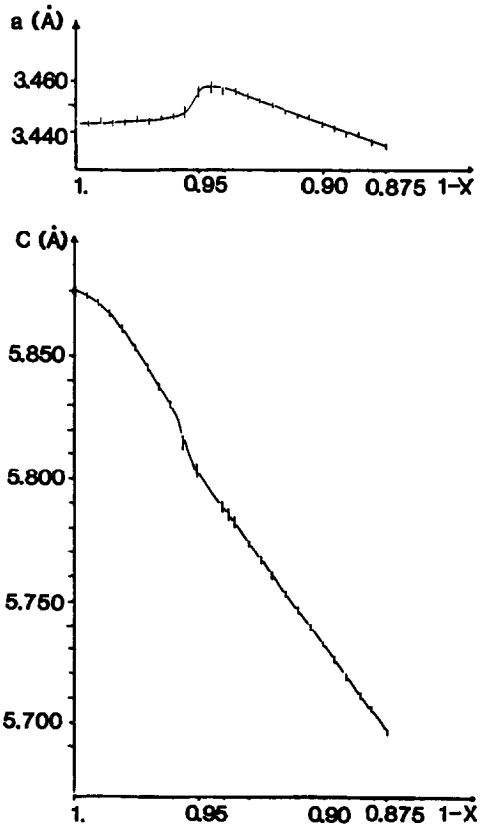

FIG. 3. Substructure a and c NiAs lattice constants of $Fe_{1-x}S$ versus $(1-x)$.

—The iron-poor side ($x_{lim} < x < 0.125$) where previous studies (*10,11*) have established that there exist various apparently hexagonal superstructures $2a,nc$ with n values that may or may not be commensurate.

Diffraction studies of crystals with x values close to $x_{lim} = 0.05$ (*7*) show that the LT $\sqrt{3}a,2c$ phase coexists with a $2a,nc$-type phase. This identification of the mixture of phases around x_{lim} suggests that the previous observations (weakening of the transition amplitude and of the $\sqrt{3}a,2c$ superstructure reflections and abnormally high hysteresis for x high) are correlated from a structural point of view with disorder phenomena induced by vacancies.

III. Crystal Growth for Compositions in the α Transition Range

(*A*) *Preparation of Off-Stoichiometric Samples*

On the basis of previous work (*12*) a first series of iron-rich crystals is grown by a transport reaction with Cl_2 as the transport agent. The temperature T_1 of the hot zone is between 630 and 860°C. Cl_2 pressure varies from 25 to 100 Torr. Hexagonal platelets or needles are formed in the cold zone with $560°C < T_2 < 800°C$.

The crystals always have a higher vacancy content than the initial powders used, and, as in previous work, it is impossible to reach the stoichiometric composition FeS. This can originate from the formation of $FeCl_2$, which crystallizes with quenching of the transport tube. Introduction of an excess of Fe or Al, which gives dissociated $AlCl_3$ if the hot zone is at $T_1 > 900°C$, does not solve the difficulty. However, experiments with Al lead to the highest iron content ($Fe_{0.985}S$) obtained so far, in a very reproducible way.

This first series of experiments allows preparation of crystals with compositions $Fe_{0.985}S$ and $Fe_{0.975}S$ in the transition range, but few are convenient for easy measurements of the transport properties.

(*B*) *Preparation of Stoichiometric FeS Samples*

To reach the FeS composition, $Fe_{0.985}S$ crystals are reduced in a current of hydrogen. Their composition is determined by reference to their T_α, and the crystallographic quality is analyzed on Weissenberg diagrams. This method gives some suitable FeS crystals, but their mosaic is appreciably dislocated. This is an inconvenience for the study of diffraction peak profiles (see Section IV), but not for the data collection necessary for structure refinements.

(*C*) *FeS Metastable Composition*

Large crystals ($400 \times 250 \times 70\ \mu^3$) for physical measurements are submitted to reduction and annealed at 1000°C for a week in an evacuated silica–glass tube. At this temperature a reorganization of the lattice by atomic diffusion in the material is expected. But after quenching, T_α has decreased to a value corresponding to $Fe_{0.993}S$. This approximate composition is given by many authors (*4,13*) as the most stoichiometric composition obtained by crystal growth. It seems to define the limit of stability of the iron-rich side of $Fe_{1-x}S$. Thus FeS crystals obtained after reduction appear to be in a nonequilibrium state. The effect of annealing is to release excess iron. The FeS crystal directly obtained by reduction has remained stable in the course of its temperature study from RT to 200°C, its initial crystallographic characteristics (intensity, peaks profiles) being unchanged at RT after heating. However, the lack of large good-quality crystals prevents the expected physical measurements and collection of monochromatic X-ray diagrams which would show the existence of some HT superstructure reflections which have not been seen before (see Section VI).

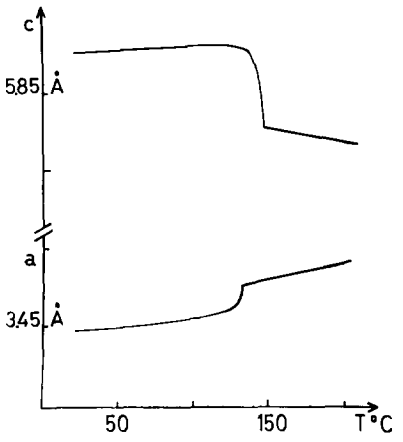

FIG. 4. Substructure a and c NiAs lattice constants versus T for the FeS crystal.

IV. X-ray Study of a Stoichiometric FeS Crystal

(A) *Lattice Constants, Intensity Ratios, and Peak Profiles*

The X-ray experiments are carried out on an automatic four-circle SYNTEX diffractometer (MoK_α) equipped with a heating device. In order to prevent oxidation, the cystals are protected by a sealed Lindemann glass tube.

Figure 4 presents the variation of the NiAs substructure lattice constants a and c with respect to T. At T_α, a and c exhibit a change, particularly prononced for c, such that $c_{HT} < c_{LT}$ and $a_{HT} > a_{LT}$.

Figure 5a shows the evolution with T of the ratio I/I_0 of the intensities measured at RT (I_0) and at T (I) of some characteristic reflections of the cells affected by the transition. Their indices are expressed with respect to the three cells studied: ideal NiAs for the substructure lattice (a,c); hexagonal $(\sqrt{3}a,2c)$ for the LT superstructure, and hexagonal $(2a,c)$ for the modification identified up to T_α. Simultaneously, at some selected temperatures, the peak profiles of these reflections indicate the correlation length in the crystal, i.e., the average length of regions with the corresponding structural order. The strongest substructure reflections $110(a,c)$ and $004(a,c)$ indicate the gradual change of the distortion from the ideal NiAs lattice in respectively, the hexagonal plane and the c direction.

From 130°C the intensity of the 121 $(\sqrt{3}a,2c)$ reflection decreases to zero at T_α = 147°C and its peak profile flattens and broadens (Figs. 5a and 5d). From the pretransition range to $T > T_\alpha$, the 110 (a,c) reflection increases, indicating the weakening of the NiAs lattice distortion in the hexagonal plane, but the 004 (a,c) reflection does not change appreciably (Fig. 5a). Their peak profiles, appreciably broadened because of the quality of the crystal, are unchanged. (Figs. 5b and 5c): The substructure lattice retains long-range order in the temperature range investigated.

In the HT range, at 156°C, the 031 $(2a,c)$ reflection intensity reaches its maximum value, and the $2a,c$ superstructure exhibits long-range order (same peak profile as that of the substructure reflections. (Figs. 5a and 5c). Its temperature range of existence is narrow. The hysteresis of the transition registered on the 031 $(2a,c)$ reflection is small: 4°C.

(B) *Weakening Process of Superstructure Reflections*

Peak profiles indicate the comparative evolution of the correlation length of the substructure and complementary structure lattices. In FeS,LT$(\sqrt{3}a,2c)$ and HT$(2a,c)$ superstructures originate from the long-range order of atomic displacements (essentially those of the heavy atoms Fe) with respect to their ideal NiAs positions. The intensity of superstructure reflections depends on the amplitude of the NiAs lattice distortion and decreases with it. In a normal crystal, where atomic shifts would be smaller but would remain ordered over a long distance (we call this a relaxed model),

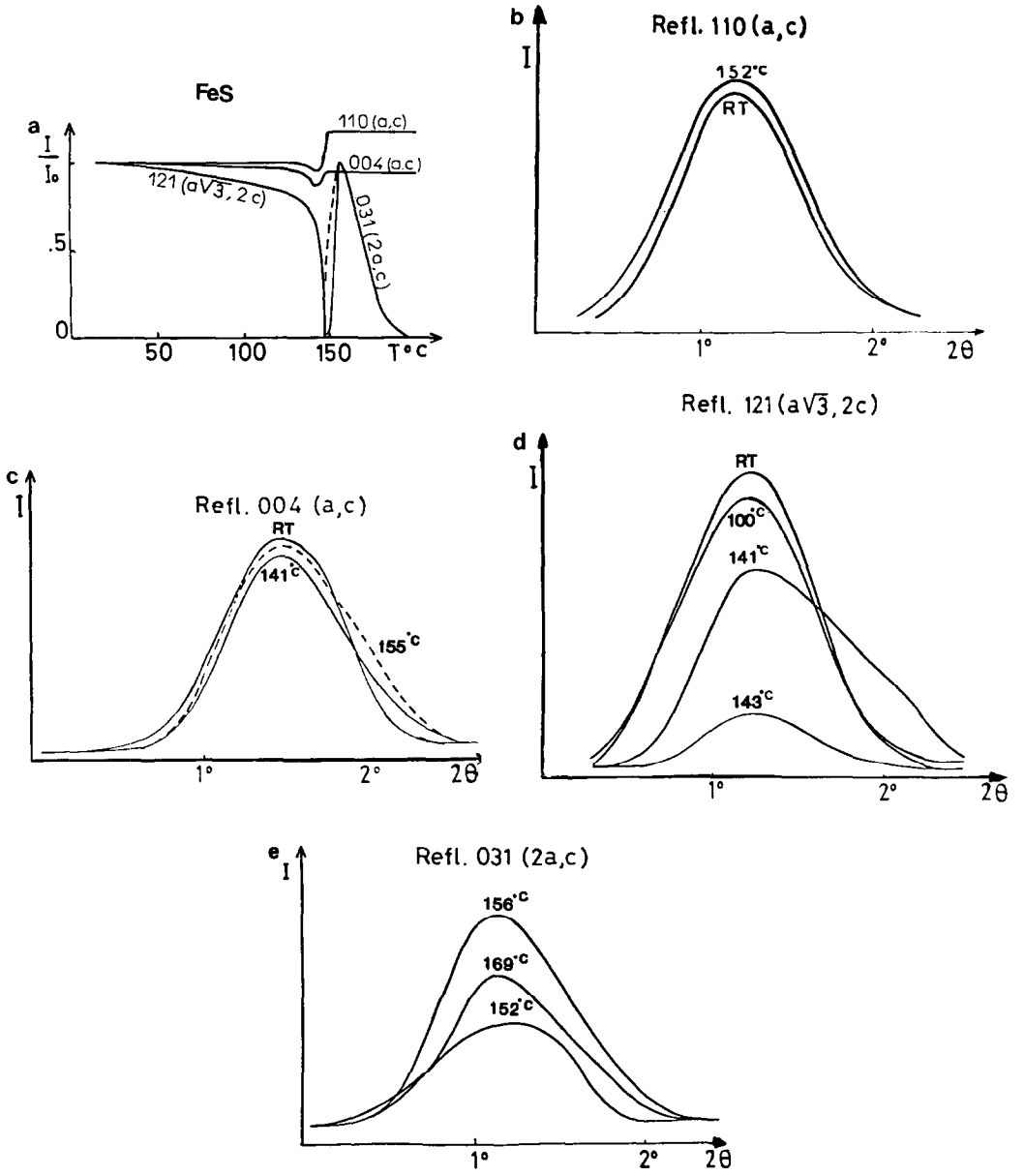

FIG. 5. (a) Relative intensity I/I_0 versus T of characteristic reflections for the three structural types affected by the transition. (I_0 measured at RT and I at T):110(a,c) and 004(a,c) from the NiAs substructure and 121($\sqrt{3}a$,$2c$) and 031($2a$,c) from respectively LT and HT superstructures. (Dotted lines: observations in the hysteresis range.) Peak profiles at various temperatures: (b) and (c): 110(a,c) and 004(a,c) substructure reflections; (d) 121 ($\sqrt{3}a$,$2c$) LT superstructure reflection; and (e) 031($2a$,c) HT superstructure reflection.

substructure and complementary structure lattices have the same correlation length. Their reflections have the same peak profile, and their intensities depend on the same number of cells: they are treated with the same scale factor during the structural refinement of this long-range ordered crystal.

In fact, we observe a temperature-dependent specific broadening of the superstructure reflections compared to those of the substructure. This shows that the correlation length of the superstructure lattice is shorter than that of the substructure lattice, and indicates the occurrence of disorder which limits the long-range order of the atomic shifts, but which does not affect the order of the average atomic positions in the substructure lattice. In this model, the superstructure lattice is limited to domains separated by disordered regions which do not contribute to the intensity of the superstructure reflections, while they do contribute to the substructure reflections. As a consequence, these two kinds of reflections must be treated with two independent scale factors (named SC) with SC (superstructure) < SC (substructure).

Final R factor analysis of refinements based upon either the relaxation model or the domain model shows that the latter gives a better representation of the main weakening process of the superstructure intensity versus T.

When materials contain vacancies or are M-substituted (M = Cr or Mn in $Fe_{1-x}M_xS$), it is easy to imagine that disordered regions are created around these constituents which act as impurities (*8*). In the LT $\sqrt{3}a,2c$ superstructure they cannot be inserted in a position of the characteristic triangular Fe^{2+} clusters of the hexagonal plane, with short distances of about 2.9 Å. Thus they locally destroy this characteristic cluster and the atomic positions relax to those of the ideal NiAs. Disordered regions appear where vacancies or M constituents segregate, but the average lattice is unmodified. For a stoichiometric FeS crystal, the formation of disordered zones originates from temperature only. They appear in a narrow temperature range below T_α as revealed by broadening of the 121 ($\sqrt{3}a,2c$) reflection associated with a decrease in its intensity.

V. Structural Analysis Versus T of the FeS LT Phase

(A) *Experimental*

The LT hexagonal superstructure $\sqrt{3}a,2c$ (space group $P\bar{6}2c$) is analyzed at room temperature and in the immediate pretransition range at 141°C. Reflections are collected on two equivalent sectors *hkl* and *khl*, between $2\theta = 0$ and 65°. After an absorption correction ($\mu = 134\ cm^{-1}$) using the analytical method (*14*), the structure factor of each independant reflection is calculated as the average of the two measurements. In each case, the whole set of independant reflections collected is used in the refinement, including those with $I = 0$. The least-square refinement program used is ORXFLS.3 (*15*).

(B) *LT FeS Structural Refinement at RT*

First, sub- and superstructure reflections are treated with the same scale factor. Following the final cycle with anisotropic temperature factors, the R^1 value is 3.1%. Refinement of the individual scale factors leaves this result unchanged and confirms the perfectly ordered description.

Table I presents the final parameters and Tables II and III selected distances. These results agree with those of Evans (*16*) on a lunar FeS crystal.

[1] The R factor used in this work is: $R = \Sigma \| F_0| - |F_c\| / \Sigma |F_0|$.

TABLE I

ATOMIC POSITIONS AND THERMAL PARAMETERS (Å² × 10⁴) IN LT FeS $\sqrt{3}a,2c$

Atoms[a]		T = RT	T = 141°C
Fe (12*i*)	x	0.3786(2)	0.3761(2)
($\frac{1}{3}$;0;$\frac{1}{8}$)	y	0.0553(2)	0.0527(2)
	z	0.1230(1)	0.1233(1)
	U_{11}	178(5)	246(6)
	U_{22}	146(5)	195(6)
	U_{33}	131(4)	197(4)
	U_{12}	84(4)	117(5)
	U_{13}	−6(4)	−10(4)
	U_{23}	−12(4)	−22(4)
S_1 (2*a*)	$x = y = z$	0.	0.
(0;0;0)			
	$U_{11} = U_{22} = 2U_{12}$	113(11)	155(11)
	U_{33}	133(15)	182(14)
	$U_{13} = U_{23}$	0.	0.
S_2 (4*f*)	x	$\frac{1}{3}$	$\frac{1}{3}$
($\frac{1}{3}$;$\frac{2}{3}$.0)	y	$\frac{2}{3}$	$\frac{2}{3}$
	z	0.0200(2)	0.0189(3)
	$U_{11} = U_{22} = 2U_{12}$	122(8)	167(8)
	U_{33}	133(11)	185(12)
	$U_{13} = U_{23}$	0.	0.
S_3 (6*h*)	x	0.6653(5)	0.6651(5)
($\frac{2}{3}$;0;$\frac{1}{4}$)	y	−0.0030(6)	−0.0027(6)
	z	$\frac{1}{4}$	$\frac{1}{4}$
	U_{11}	105(10)	159(11)
	U_{22}	109(10)	161(10)
	U_{33}	136(8)	200(7)
	U_{12}	51(9)	76(10)
	$U_{13} = U_{23}$	0.	0.
Sub-[Sc(1)] and superstructure [Sc(2)] scale factors		Sc(1) = Sc(2)	(Sc(1)-Sc(2))/Sc(1) = 8.8(±1.6)%
Final R		3.1%	3.6%
Number of reflections and variables parameters		286; 22	288; 23
			If Sc(1) = Sc(2), R' = 4.2%[b]
Sub- and superstructure partial R with No. of reflections		R_{sub} = 3% (55)	R_{sub} = 2.3% (55)
		R_{sup} = 3.2% (231)	R_{sup} = 4.8% (233)
Substructure lattice parameters (in Å)	a	3.444(1)	3.455(1)
	c	5.878(1)	5.871(1)

Note. SG = $P\bar{6}2c$.

[a] Ideal NiAs position in the $\sqrt{3}a,2c$ cell are noted in brackets.

[b] Hamilton's test is significant with R'/R = 1, 167 > R_{tab} = 1.016 for (1;250;0.5%) parameters.

TABLE II

CHARACTERISTIC Fe–Fe AND Fe–S DISTANCES (Å) IN LT FeS $\sqrt{3}a,2c$: EVOLUTION WITH T

		T = RT		T = 141°C	
Distances	Multiplicity		Ideal NiAs value		Ideal NiAs value
⟨Fe–Fe⟩					
Along c					
B	1	2.949	c/2=	2.947	c/2=
C	1	2.985	2.939	2.974	2.935
Average ⟨Fe–Fe⟩		2.967		2.960	
In basal plane					
A	2	2.925	a=	2.962	a=
	2	3.660	3.444	3.656	3.455
	2	3.802		3.799	
Average ⟨Fe–Fe⟩		3.462		3.472	
⟨Fe–S⟩					
Fe–S_3	1	2.356		2.361	
Fe–S_2	1	2.383		2.390	
Fe–S_3	1	2.422	2.473	2.426	2.476
Fe–S_2	1	2.507		2.513	
Fe–S_1	1	2.561		2.560	
Fe–S_3	1	2.721		2.713	
Average ⟨Fe–S⟩		2.493		2.494	

Note. SD ∠ 0.005 Å.

TABLE III

S–S DISTANCES (Å) IN LT FeS $\sqrt{3}a,2c$: EVOLUTION WITH T

Distances	Multiplicity	T = RT	T = 141°C
In basal plane			
S_1–S_2	6	3.452	3.462
S_2–S_2	3	3.476	3.483
S_3–S_3	2	3.421	3.433
S_3–S_3	2	3.442	3.457
S_3–S_3	2	3.467	3.476
Average ⟨S–S⟩		3.453	3.463
Ideal NiAs			
value = a		3.444	3.455
Along c			
S_1–S_3	6	3.548	3.550
S_2–S_3	3	3.348	3.360
S_2–S_3	3	3.753	3.741
Average ⟨S–S⟩		3.549	3.550
Ideal NiAs			
value		3.548	3.549

Note. SD ∠ 0.005 Å.

(C) *LT FeS Structural Refinement at 141°C, in the Prestransition Range*

When the two kinds of reflections are used in the refinement with a common scale factor the final R value is 4.2% but is lowered to 3.6% when individual scale factors are refined. Hamilton's test (*17*) confirms that with introduction of a supplementary parameter, this R change is significant (Cf, Table I). The small relative difference of 8.8 (± 1.6)% between the scale factors reflects the small proportion of disordered regions in the stoichiometric crystal some few degrees before T_α. Table I presents the final parameters and Tables II and III selected distances.

VI. Structural Analysis of FeS HT Phase

(A) *Previous Work*

The structural change at T_α was first supposed to give an ideal NiAs HT phase. But studies of meteoritic FeS (*18,19*) report the existence of a transitional phase with lattice constants $2a,2a,c$ at $T > T_\alpha$. Extensive classical X-ray study of a synthetic crystal was performed by King and Prewitt (*6*) above T_α, at 175°C. Diffuse extra reflections on the hkl and $hk2$ levels of the subcell lattice suggest the existence of a hexagonal superstructure $2a,c$. But their apparent extinction for $l = 0$ is inconsistent with a hexagonal space group and leads the authors to adopt a twinned model with a *MnP*-type cell. But their refinement with a final R factor equal to 14.5% does not give a satisfactory answer to the question of the real nature of HT FeS.

(B) *Evidence for the Hexagonal 2a,c Form of HT FeS*

A stoichiometric FeS crystal is analyzed some few degrees above the transition. Precession diagrams are performed with monochromatic radiation (MoK_α) from a bent graphite crystal. Beside the substructure reflections, the $hk1$ level of the NiAs subcell exhibits extra diffuse reflections which can be indexed in an hexagonal lattice $2a,c$. But, as for King and Prewitt, it is impossible to identify such extra reflections on the $hk0$ level. Experimental difficulties (quality of the crystal, important background created by the thermal diffusion and the glue) prohibit observation of the systematic extinction h and/or $k = 2n + 1$, $l = 0$ of superstructure reflections from a hexagonal lattice $2a,c$. However, this kind of superstructure cell has already been signaled as resulting from a NiAs lattice distortion in the low-temperature phase of NbS (*20*).

The search for these reflections is performed on the diffractometer at $T = 156$°C, which corresponds to the maximum intensity of the strong noncontroversial superstructure reflection 031 ($2a,c$). The data are collected in four equivalent sectors of reciprocal space of the $2a,c$ lattice. This detects weak superstructure $2a,c$ reflections on $l = 2n$ levels. In particular, when $l = 0$, they just emerge from the background and this explains why they are hardly observable. Thus, evidence of very weak but measurable extra reflections on the $hk0$ level challenges the *MnP* model and suggests an hexagonal $2a,c$ description.

(C) *Refinement of the 2a,c Superstructure at T = 156°C*

After absorption correction, the four equivalent sets of reflections collected between $2\theta = 0$ and 65° are reduced to 197 independant reflections with a structure factor taken as the average of the equivalent data. The relation $I(hkl) = I(khl) = I(hk\bar{l})$ and the systematic extinction rule $hh(2\bar{h})l, l = 2n + 1$ suggest three possible hexagonal space groups: $P6_3/mmc$;$P\bar{6}2c$; and $P6_3mc$. Only the last accounts for the intensity distribution of the superstructure reflections. Least-square refinement is performed using the whole set of reflections,

TABLE IV

ATOMIC POSITIONS AND THERMAL PARAMETERS (Å^2 × 10^4) IN HT FeS $2a,c$ (SG = $P6_3mc$)

Atomic parameter[a] ($y = 2x$)		T = 156°C	T = 180°C
	x	0.5098(2)	0.511(1)
	z	0	0
Fe_1 (6c)	U_{11}	539(12)	566(21)
	$U_{22} = 2U_{12}$	429(15)	536
($\frac{1}{2}$;0;0)	U_{33}	206(11)	189(15)
	$U_{13} = 0.5U_{23}$	−6(13)	−20(18)
Fe_2 (2a)	x	0	0
	z	−0.006(1)	−0.008(2)
(0;0;0)	$U_{11} = U_{22} = 2U_{12}$	577(18)	550(31)
	U_{33}	125(20)	215(46)
	$U_{13} = U_{23}$	0	0
	x	0.1667(4)	0.1663(9)
	z	0.240(2)	0.245(3)
S_1 (6c)	U_{11}	320(15)	400(27)
	$U_{22} = 2U_{12}$	315(21)	360(37)
($\frac{1}{6}$;$\frac{1}{3}$;$\frac{1}{4}$)	U_{33}	206(19)	211(24)
	$U_{13} = 0.5U_{23}$	−1(7)	0(1)
S_2 (2b)	x	$\frac{1}{3}$	$\frac{1}{3}$
	z	0.761(2)	0.7656(40)
($\frac{1}{3}$;$\frac{2}{3}$;$\frac{3}{4}$)	$U_{11} = U_{22} = 2U_{12}$	218(18)	157(26)
	U_{33}	323(70)	340(91)
	$U_{13} = U_{23}$	0	0
Sub [Sc(1)] and superstructure [Sc(2)] scale factors		Sc(1) = Sc(2)	(Sc(1) − Sc(2))/Sc(1) = 57(±6)%
Final R		6.0%	6.8%
Number of reflections		197	196
Partial R for sub- and superstructure, with the number of reflections in parenthesis		R_{sub} = 4.3% (55) R_{sup} = 12% (142)	R_{sub} = 3.7% (55) R_{sup} = 16.3% (141)
Substructure lattice constants (in Å)		a = 3.479(1) c = 5.824(1)	a = 3.487(1) c = 5.821(1)

[a] Ideal NiAs positions in the $2a,c$ cell are noted in brackets.

including those with $I = 0$. Taking into account the long-range order of the $2a,c$ superstructure at T = 156°C, sub- and superstructure reflections are treated with a common scale factor. After refinement of the anisotropic temperature factor the final R value is 6.0%. Its decomposition into partial Rs gives 4.3% for the 55 substructure reflections and 12% for the 142 superstructure reflections, which is a satisfactory result, given the number of weak reflections. Final parameters and selected distances are presented in Tables IV, V, and VI.

(D) *Discussion of the MnP Model of the HT Phase of FeS*

The final refinement of the hexagonal $2a,c$ description is already more satisfactory than the previous result of King and

TABLE V

CHARACTERISTIC Fe–Fe AND Fe–S DISTANCES (Å) IN HT FeS $2a,c$: EVOLUTION WITH T

Distances	Multiplicity	T = 156°C	Ideal NiAs value	T = 180°C	Ideal NiAs value
⟨Fe–Fe⟩					
Along c					
Fe_1–Fe_1 B	2	2.922	$c/2$=	2.922	$c/2$=
Fe_2–Fe_2 C	2	2.912	2.912	2.910	2.910
Average ⟨Fe–Fe⟩		2.917		2.916	
Basal plane					
Fe_1–Fe_1 A	2	3.275	a=	3.265	a=
Fe_1–Fe_1	2	3.683	3.479	3.708	3.487
Fe_1–Fe_2 D	2	3.482		3.489	
Average ⟨Fe–Fe⟩		3.480		3.487	
⟨Fe–S⟩					
Fe_1–S_2	1	2.425		2.438	
Fe_1–S_1	2	2.470		2.455	
Fe_1–S_1	2	2.499	2.481	2.522	2.484
Fe_1–S_2	1	2.543		2.539	
Average ⟨Fe_1–S⟩		2.484		2.489	
Fe_2–S_1	3	2.471		2.472	
Fe_2–S_1	3	2.492	2.481	2.489	2.484
Average ⟨Fe_2–S⟩		2.481		2.481	

Note. SD ∠ 0.10 Å at T = 156°C and ∠ 0.02 Å at T = 180°C.

TABLE VI

S–S DISTANCES (Å) IN HT FeS $2a,c$: EVOLUTION WITH T

Distance	Multiplicity	T = 156°C	T = 180°C
In basal plane			
S_1–S_1	2	3.478	3.479
S_1–S_1	2	3.480	3.494
S_1–S_2	2	3.481	3.489
Average ⟨S–S⟩		3.480	3.487
Ideal NiAs value = a		3.479	3.487
Along c			
S_1–S_2	1	3.441	3.443
S_1–S_1	4	3.538	3.536
S_1–S_2	1	3.635	3.641
Average ⟨S–S⟩		3.538	3.538
Ideal NiAs value		3.537	3.539

Note. SD ∠ 0.01 Å at T = 156°C, ∠ 0.02 Å at T = 180°C.

Prewitt (R = 14.5%). To explain the apparent extinction rule h and/or $k = 2n + 1$ on the $hk0$ level of a $(2a,c)$ lattice, these authors describe the crystal as a twin made of three orthorhombic domains related by a 60° rotation around the c axis of the NiAs substructure cell. In each domain the orthorhombic *MnP*-type cell is supposed to be a slight deformation of the orthohexagonal cell with $(c,a, \sqrt{3}a)$ lattice constants and space group *Pnma*. But two arguments contest this description:

—A deformation of the orthohexagonal cell would give broadening or splitting of the substructure reflections. This was not observed in the previous HT studies and on X-ray powder diagrams obtained between T_α and the Néel temperature = 327°C.

—Based on the set of reflections collected at 156°C in the $2a,c$ lattice description, the *MnP* cell refinement is performed after transformation of the indices. According to the evenness of its indices in the $2a,c$ description, each superstructure reflection belongs to one of the three domains. But each substructure spot results from the superposition of three independent substructure reflections, from each of the twin domains. Using the apparent hexagonal symmetry, the whole set of 142 $(2a,c)$ superstructure reflections is expressed as belonging to the same orthorhombic domain, and the intensities of the diffraction spots from the fundamental lattice are calculated as the sum of the three *MnP* substructure reflections related by the 60° rotation.

The initial atomic positions introduced for the *MnP* cell refinement are those given by King and Prewitt. Two independant scale factors are introduced: One for the substructure reflections and the other common to the three sets of superstructure reflections. After a few cycles, the two become equal. This indicates that the three domains of the hypothetical tritwinned model have the same volume, as expected from the hexagonal symmetry observed. With anisotropic thermal parameters for each atom, the final R value is 7.39% for the whole set of 197 reflections, including those with $I = 0$ and the 23 weak superstructure reflections from the $(hk0)_{2a,c}$ level supposed to be forbidden in the *MnP* model.

This result is already more precise than the *MnP* model refinement of King and Prewitt (R = 14.5%), but it does not rule out the hexagonal $2a,c$ model. Its final R value of 6.0% (for 19 variable parameters) shows a significant decrease compared to an R of 7.39% for 15 parameters of the *MnP* twinned model. This is confirmed by Hamilton's test ($R/R' = 1.23 > R_{tabl}$ (4; 120; 0.005) = 1.063, for 197 reflections).

The absence of distortion of the substructure cell and the satisfactory refinement in the hexagonal $2a,c$ description lead to rejection of the conclusions of King and Prewitt.

Examination of the list of observed and calculated $F^{(2)}$ from the refinement of the $2a,c$ cell justifies the difficulty in observing its reflections h and/or $k = 2n + 1$, $l = 0$ when the usual X-ray or electron diffraction techniques are used. The calculated Fs are very weak. Moreover, these values are for the long-range ordered $2a,c$ superstructure, at T = 156°C. But King and Prewitt carried out their study at T = 175°C, in a temperature range where the superstructure reflections are weaker.

(E) *Refinement of the 2a,c Superstructure at T* = 180°C

At T = 180°C, the $2a,c$ superstructure is limited to short-range ordered domains. The data are collected in four equivalent sectors of reciprocal lattice, between $2\theta = 0$ and 65°. After the absorption correction, the averaged structure factors of the whole

[2] Lists of observed and calculated structure factors of the refinements presented in this paper are available on request from the authors.

set of the 196 independent reflections are used in the refinement. The first cycles are based upon atomic parameters from the previous structural analysis, and sub- and superstructure reflections are used with independant scale factors. In the final cycle, anisotropic temperature factors are refined. But the shift of Fe_1 atom in the b direction from its ideal NiAs position is described with comparable magnitude either by the positional parameter $x = \frac{1}{2} + \varepsilon$, ($y = 2x$) or the anisotropic temperature factor component β_{22}. They are strongly correlated and cannot be refined independently. Thus, based on the results of the refinement at $T = 156°C$ where the components β_{11} and β_{22} have close values, the final cycles are performed with the constraint: $\beta_{11} = \beta_{22}$. Under these conditions, the final R value is 6.8%, and the relative difference between sub- and superstructure scale factors is 57 (±6)%. Table IV presents the final parameters and Tables V and VI selected distances.

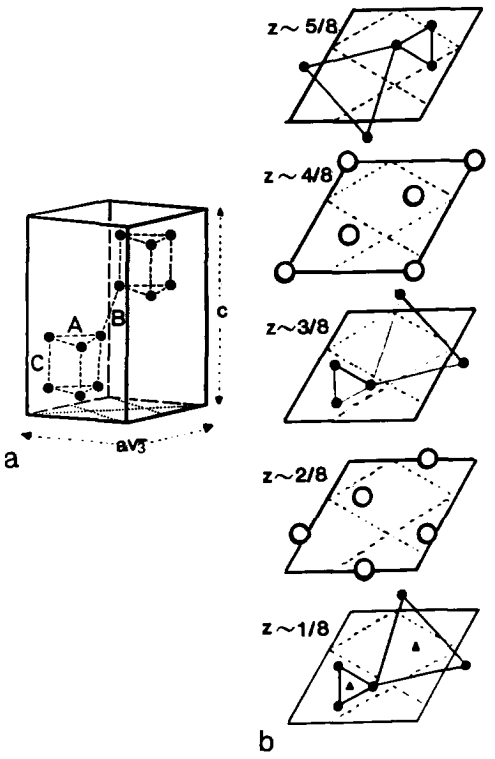

FIG. 6. (a) Schematic cationic lattice in the LT $\sqrt{3}a,2c$ cell of FeS, with characteristic Fe–Fe distances. (b) Alternation of iron (solid circles) and sulfur (open circles) planes in the c direction. In metallic planes, tight and expanded Fe triangular clusters are represented. Ideally NiAs positions of Fe atoms lie at the origin of the substructure cell, in dotted lines.

VII. Comparative Description of LT and HT Cells of FeS

In an ideal NiAs cell (Fig. 1), there are two kinds of metal–metal distances. In the hexagonal plane, each M atom on the six-fold axis has six neighbors at a distance which is the a lattice constant of the cell. This long distance corresponds to the S^{2-} diameter, about 3.45 Å. Along the c axis, M atoms form an infinite chain with short M–M distance equal to half the c lattice constant, i.e., 2.9 Å in the case of FeS.

Figures 6a, 6b, 7a, and 7b present the LT and HT cells of FeS. Comparison of them shows that the LT $\sqrt{3}a,2c$ cell corresponds to the strongest distortion of the ideal NiAs lattice. Fe atoms distributed on one site undergo important shifts from their ideal NiAs positions, mainly in the hexagonal plane, where they form a succession of tight and distended triangular clusters. In the c direction, they form triangular prisms alternating along the six-fold axis, and this destroys the infinite chain of Fe atoms which would extend along the c axis in an ideal NiAs cell.

In the HT $2a,c$ cell, Fe atoms are located on two independent sites:

—Fe_2 occupies an ideal NiAs position on the six-fold axis and preserves the infinite chain along the c axis.

—In the hexagonal plane, Fe_1 is engaged in a triangular cluster centered on the three-fold axis, but here the clusters form a helix around the six-fold axis.

Already, the existence of the infinite chain of Fe atoms makes the HT $2a,c$ cell

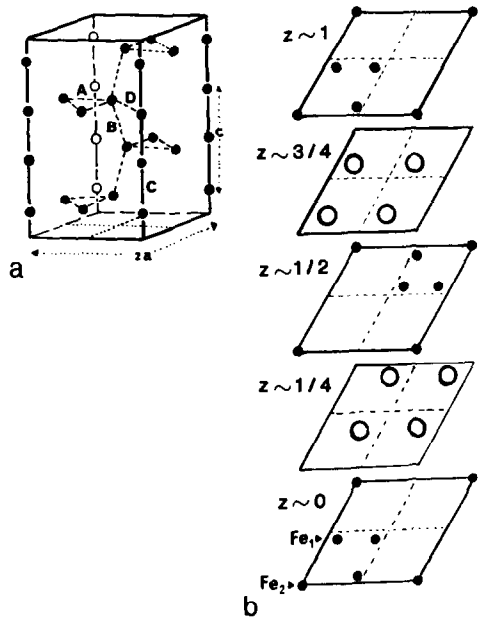

FIG. 7. (a) Schematic cationic lattice in the hexagonal $2a,c$ HT modification of FeS, with characteristic Fe–Fe distances. (b) Alternation of iron (solid circles) and sulfur (open circles) planes in the c direction. Ideally NiAs positions of Fe atoms lie at the origin of the substructure cell, in dotted lines.

intermediate between the LT $\sqrt{3}a,2c$ and that of the ideal NiAs. This is confirmed by comparing the M–M distances. In the two cells, homologous Fe–Fe distances are named with the same letter, with the cell to which each refers in parenthesis.

$A(\sqrt{3}a,2c)$ and $A(2a,c)$ are the distances in the triangular clusters of the hexagonal plane. But the $D(2a,c)$ distance between independant Fe_1 and Fe_2 atoms exists only in the HT modification. The ideal NiAs value of these distances is a, the NiAs cell lattice constant.

$B(\sqrt{3}a,2c)$ is the distance between alternated triangular prisms and $B(2a,c)$ the distance between alternating triangular clusters. In the LT cell, $C(\sqrt{3}a,2c)$ is the height of the prisms along the c direction, but $C(2a,c)$ is the Fe–Fe distance in the infinite metallic chain which remains in the HT cell. Ideal NiAs values of B and C distances are $c_{NiAs}/2$.

In FeS at RT, $A(\sqrt{3}a,2c)$ is the shortest Fe–Fe distance (2.92 Å), while it is normally the longest in an ideal NiAs cell. This points out the important distortion of the NiAs lattice at the origin of the LT superstructure. By comparison, the $A(2a,c)$ distance is much greater (3.27 Å) and the $D(2a,c)$ distance is close to its ideal value a. This makes the HT $2a,c$ modification a slight distortion of the pure NiAs lattice. In the HT cell, one returns to the characteristic distsribution of two kinds of Fe–Fe distances of the ideal cell:

—Long distances in the hexagonal plane: $A(2a,c)$ and $D(2a,c)$.

—Short distances among the two kinds of Fe chains in the c direction: $C(2a,c)$ along the six-fold axis and $B(2a,c)$ in the zigzag chain along the axis of the triangular cluster helix.

In the HT cell, the Fe–Fe distances do not change significantly when T increases. In contrast, in the LT modification, $A(\sqrt{3}a,2c)$ increases with T (from 2.92 to 2.96 Å), which indicates that Fe atoms draw nearer to their ideal positions. As a consequence of the relaxation of this displacive superstructure, $C\sqrt{3}a,2c)$ decreases slightly (but $B(\sqrt{3}a,2c)$ does not change significantly), and the distortion from the ideal sulfur coordination of Fe atoms is attenuated. However, the average Fe–S distances remain unchanged, but they have higher values than in an ideal NiAs cell.

As the HT $2a,c$ cell is a weak NiAs lattice distortion which concerns only three of the four Fe atoms, one observes that the S_6 octahedral coordination of each cation is more regular than that in the LT cell, with average Fe–S distances close to their ideal value. The *hcp* sulfur lattice is scarcely modified: Among the two independent S

positions, one remains on the six-fold axis, while the other is slightly shifted.

The lattice constant change at the transition, with a strong decrease in c and a smaller increase in a for $T > T_\alpha$, makes the HT cell flatter than the LT cell. This results in a reduction of the difference between the average S–S distances along the c direction and in the basal plane. This difference is about 0.09 Å in the LT $\sqrt{3}a,2c$ cell and 0.05 Å in the HT $2a,c$ cell.

VIII. Conclusion

The α transition is, from a structural point of view, a change from a large to a smaller deformation of the ideal NiAs lattice, which makes the HT cell intermediate between the LT $\sqrt{3}a,2c$ and the pure NiAs cells. In the pretransition range, T influences the formation of disordered zones, associated with the relaxation of the NiAs lattice distortion in the domains where the LT modification is still present.

The question remains about the mechanism of weakening of the HT $2a,c$ superstructure, which makes the structure purely NiAs (a,c) for $T > 200$°C. This displacive superstructure originates from a weak shift in the hexagonal plane of one of the four Fe atoms at the origin of a pure NiAs cell. This shift is described by one of the six vectors **S** lying in the mirror m of the 6c position of the Fe_1 atom of the $2a,c$ cell. At high temperature, we can suppose there is an easy interchange between the six possible vectors **S**, giving a dynamical superstructure $2a,c$, with cells which differ only by a change of their origin, and explain the break of the correlation length. The time-averaged position of these Fe atoms is ideal NiAs, and the superstructure is transparent to X-ray analysis.

We have tried to verify this assumption using a $Fe_{1-x}Mn_xS$ crystal with a very low substitution rate $x = 5 \times 10^{-3}$. Its effect is to preserve the characteristics of a purely FeS crystal (*8*), but to give single crystals with a better quality mosaic. Reflections of the ideal NiAs lattice of this crystal are collected at 200°C from $2\theta = 0°$ to 120°C and corrected for absorption. This dynamical delocalization of atoms of an ideal NiAs cell is analogous to thermal vibration in an anharmonic potential. Refinement of such a model leads to sixth order tensors that describe the thermal motion of each atom. The probability density function corresponding to anharmonicity is calculated using Hermite polynomial expansion, and its Fourier transform calculated to give electron density maps in the (a,c) cell (*21*). But these maps give no evidence for Fe (or S) atom delocalization with respect to an ideal NiAs lattice. So, if the previous mechanism of range order breaking of the HT $2a,c$ superstructure is true, the shifts of the atoms are smaller than those originating from HT thermal motion.

References

1. M. G. Townsend, J. R. Gosselin, R. J. Tremblay, and A. H. Webster, *J. Phys. (Paris)* **37** (Suppl. No 10), C4 11–16 (1976).
2. J. M. D. Coey, H. Roux-Buisson, and R. Brusetti, *J. Phys. (Paris)* **37** (Suppl. No. 10), C4 7–10 (1976).
3. W. Moldenhauer and W. Bruckner, *Phys. Status Solidi A* **34,** K565–571 (1976).
4. H. Roux-Buisson, Thèse d'Etat, Université Grenoble I (1980).
5. E. F. Bertaut, *Bull. Soc. Fr. Mineral Cristallogr.* **79,** 276–292 (1956).
6. H. E. King, Jr, and C. T. Prewitt, *Acta. Crystallogr. B* **38,** 1877–1887 (1982).
7. F. Keller-Besrest and G. Collin, submitted for publication.
8. G. Collin, M. F. Gardette, G. Keller, and R. Comes, *J. Phys. Chem. Solids* **46**(7), 809–821 (1985).
9. G. Collin, M. F. Gardette, and R. Comes, *J. Phys. Chem. Solids* **48**(9), 791–802 (1987).
10. H. Nakazawa and N. Morimoto, *Mater. Res. Bull.* **6,** 345–358 (1971).
11. F. Keller-Besrest, Thèse d'Etat, Université Paris VI (1984).

12. C. Bernard, G. Fourcaudot, and J. Mercier, *J. Cryst. Growth* **35,** 192–200 (1976).
13. J. L. Horwood, M. G. Townsend, and A. H. Webster, *J. Solid State Chem.* **17,** 35–42 (1976).
14. J. D. Meulenaer and H. Tompa, *Acta Crystallogr.* **19,** 1014 (1965).
15. W. R. Busing, K. O. Martin, and H. A. Levy, "ORXFLS. 3," April 1971 Version, National Laboratory, Oak Ridge, TN.
16. H. T. Evans, *Science* **167,** 621–623 (1970).
17. "International Tables for X-Ray Crystallography," Vol. IV, p. 292 (1974).
18. A. Putnis, *Science* **186,** 439–440 (1974).
19. J. Topel-Schadt, and W. F. Muller, *Phys. Chem. Miner.* **8,** 175–179 (1982).
20. F. Kadijk and F. Jellinek, *J. Less-Common Met.* **19,** 421–430 (1969).
21. C. K. Johnson and H. A. Levy, "International Tables for X-Ray Crystallography," Vol. IV, p. 313 (1974).